X-ray Crystal Structure and ^{31}P NMR Solution Studies of $[Ir_2(dimen)_4(PPh_3)Au(PPh_3)](PF_6)_3$ (dimen = 1,8-Diisocyano-*p*-menthane). Observation of Partial Site Preference in the Formation of "Outside" Ag and Au Adducts

Andrew G. Sykes and Kent R. Mann*

Contribution from the Department of Chemistry, University of Minnesota, Minneapolis, Minnesota 55455. *Received January 30, 1990*

Abstract: The reaction of $[M(PPh_3)_2](PF_6)$ (M = Ag, Au) with $[Ir_2(dimen)_4](PF_6)_2$ leads to the formation of heteronuclear complexes of the general formula $[Ir_2(dimen)_4(PPh_3)M(PPh_3)](PF_6)_3$. Recrystallization of the Au complex from CH_3CN/ether solution afforded crystals of $[Ir_2(dimen)_4(PPh_3)Au(PPh_3)](PF_6)_3 \cdot CH_3CN$ ($AuIr_2C_{86}H_{105}F_{18}N_9P_5$) that were the subject of an X-ray crystal structure characterization. The complex crystallizes in the monoclinic space group *Cc* (No. 9) with $Z = 4$; $a = 24.79$ (2), $b = 15.792$ (6), $c = 23.307$ (6) Å; $\beta = 94.15$ (4)°; $V = 9102$ Å^3. At convergence, $R = 0.055$ and $R_w = 0.064$ for 6382 observed reflections. The crystal contains tripositive cations with a $Au(PPh_3)^+$ unit occupying one of the $[Ir_2(dimen)_4]^{2+}$ axial sites and a PPh_3 in the second axial position. The PPH_3-Ir_2-$Au(PPh_3)$ moiety features a two-electron two-center Ir-Au bond with a Ir-Au distance of 2.607 (2) Å. Au-P and Ir-P bond distances in the structure are 2.199 (7) and 2.482 (7) Å, respectively. The $Ir(CNR)_4$ planes are nearly staggered with a twist angle of 39°. The Ir-Ir separation is 2.986 (2) Å. From $^{31}P\{^1H\}$ NMR solution studies and homonuclear $^{31}P\{^1H\}$ δ/J-resolved NMR spectroscopy, a nonstatistical distribution of five out of six different geometric isomers is present in CH_2Cl_2 solutions of both the Ag^+ and Au^+ complexes.

Introduction

During the past[1] several years, a considerable expansion of the chemistry of gold and mixed-metal gold cluster compounds has occurred. The expansion has been driven by the exposition of the isolobal relationship between $Au(PR_3)$ fragments and H, CH_3, and $Mn(CO)_5$ moieties[2] and the potential uses of mixed-metal gold clusters as catalytic precursors.[2-4] Recent reviews of mixed-metal gold chemistry[5-8] suggest a distinction be made between (a) uncharged mixed-metal gold cluster compounds containing primarily carbon monoxide ligands and (b) those compounds containing principally phosphine ligands.

The mixed-metal Ir-$Au(PR_3)$ complexes that have been reported are primarily limited to the second classification.[9-16] Complexes of this type frequently feature the $Au(PR_3)$ fragment bridging other iridium or gold atoms in the complexes,[10,12,14,15] or the Ir-Au bond is bridged by hydrides.[9,11,16] There is only one example of an Ir-$Au(PR_3)$ complex in the literature with an unsupported Ir-Au bond that has been characterized by X-ray crystallography.[13] The crystal structure of $[Ir(dppe)_2Au(PPh_3)]^{2+}$ contains a square-pyramidal iridium complex with the $Au(PPh_3)^+$ unit in the apical position. Other examples of two-center two-electron M-$Au(PPh_3)$ complexes include $(OC)_4CoAu(PPh_3)$[17] (which has also been characterized crystallographically), $[PtMe_2(bpy)Au(PPh_3)]NO_3$[18] (no X-ray characterization), and two other proposed Ir-$Au(PPh_3)$ complexes characterized by solution ^{31}P NMR.[11]

In contrast to Ir-$Au(PR_3)$ chemistry, most of the M-$Ag(PR_3)$ complexes previously described contain bridging $Ag(PR_3)$ units,[9,19-21] although a particularly interesting terminal $Ag(PPh_3)$ unsupported by additional covalent bonds is found in the platinum complex $(C_6F_5)_3(SC_4H_8)Pt$-$Ag(PPh_3)$.[22]

In this paper, we report the addition of $[M(PPh_3)_2](PF_6)$ (M = Ag, Au) to solutions of $[Ir_2(dimen)_4](PF_6)_2$ (dimen = 1,8-diisocyano-*p*-menthane; Figure 1) to yield heteronuclear compounds of the general type $[Ir_2(dimen)_4(PPh_3)M(PPh_3)](PF_6)_3$. We compare these "outside" adducts (schematically represented by P-Ir-Ir-Ag-P^{3+} and P-Ir-Ir-Au-P^{3+}) to the previously reported "inside" adduct $[AgIr_2(dimen)_4(PPh_3)_2]^{3+}$ (represented by P-Ir-Ag-Ir-P^{3+}).[23] To make these comparisons, the axial site preference of the $M(PPh_3)^+$ unit has been investigated by ^{31}P NMR spectroscopy, and the structure of the representative Au complex has been determined by a single-crystal X-ray diffraction analysis.

Experimental Section

General Considerations. $AgPF_6$, $Au(PPh_3)Cl$, and triphenylphosphine were purchased from Aldrich Chemical Co. All solvents were ACS reagent grade and used without further purification. $[Ir_2(dimen)_4]^{2+}$ has previously been reported as the tetraphenylborate[24] and hexafluoro-

(1) (a) Schmidbaur, H. *Angew. Chem., Int. Ed. Engl.* **1976**, *15*, 728. (b) Schmidbaur, H.; Wohlleben, A.; Wagner, F.; Orama, O.; Huttner, G. *Chem. Ber.* **1977**, *110*, 1748. (c) Schmidbaur, H.; Dash, K. C. *Adv. Inorg. Chem. Radiochem.* **1982**, *25*, 239. (d) Usón, R.; Laguna, A.; Laguna, M.; Fernandez, E.; Villacampa, M. D.; Jones, P. G.; Sheldrick, G. M. *J. Chem. Soc. Dalton Trans.* **1983**, 1679. (e) Murray, H. H.; Briggs, D. A.; Garzón, G.; Raptis, R. G.; Porter, L. C.; Fackler, J. P., Jr.; *Organometallics* **1987**, *6*, 1992. (f) Schmidbaur, H.; Graf, W.; Müller, G. *Angew. Chem., Int. Ed. Engl.* **1988**, *27*, 417. (g) King, C.; Heinrich, D. D.; Garzón, G.; Wang, J.-C.; Fackler, J. P., Jr. *J. Am. Chem. Soc.* **1989**, *111*, 2300.

(2) Hoffmann, R. *Angew. Chem., Int. Ed. Engl.* **1982**, *21*, 71.

(3) (a) Braunstein, P.; Rose, J. *Gold Bull.* **1985**, *18*, 17. (b) Schwank, J. *Gold Bull.* **1985**, *18*, 1.

(4) Sinfelt, J. H. *Bimetallic Catalysis*; Wiley: New York, 1983; Chapter 2.

(5) Mueting, A. M.; Bos, W.; Alexander, B. D.; Boyle, P. D.; Casalnuovo, J. A.; Balaban, S.; Ito, L. N.; Johnson, S. M.; Pignolet, L. H. *New J. Chem.* **1988**, *12*, 505.

(6) Jones, P. G. *Gold Bull.* **1986**, *19*, 46.

(7) Braunstein, P.; Rose, J. *Gold Bull.* **1985**, *18*, 17.

(8) Hall, K. P.; Mingos, D. M. P *Prog. Inorg. Chem.* **1984**, *32*, 237.

(9) Albinati, A.; Ankin, C.; Janser, P.; Lehner, H.; Matt, D.; Pregosin, P. S.; Venanzi, L. M. *Inorg. Chem.* **1989**, *28*, 1105.

(10) Albinati, A.; Demartin, F.; Janser, P.; Rhodes, L. F.; Venanzi, L. M. *J. Am. Chem. Soc.* **1989**, *111*, 2115.

(11) Alexander, B. D.; Johnson, B. J.; Johnson, S. M.; Casalnuovo, A. L.; Pignolet, L. H. *J. Am. Chem. Soc.* **1986**, *108*, 4409.

(12) Casalnuovo, A. L.; Casalnuovo, J. A.; Nilsson, P. V.; Pignolet, L. H. *Inorg. Chem.* **1985**, *24*, 2554.

(13) Casalnuovo, A. L.; Laska, T.; Nilsson, P. V.; Olofson, J.; Pignolet, L. H. *Inorg. Chem.* **1985**, *24*, 233.

(14) Casalnuovo, A. L.; Laska, T.; Nilsson, P. V.; Olofson, J.; Pignolet, L. H.; Bos, W.; Bour, J. J.; Steggerda, J. J. *Inorg. Chem.* **1985**, *24*, 182.

(15) Casalnuovo, A. L.; Pignolet, L. H.; van der Velden, J. W. A.; Bour, J. J.; Steggerda, J. J. *J. Am. Chem. Soc.* **1983**, *105*, 5957.

(16) Lehner, H.; Matt, D.; Pregosin, P. S.; Venanzi, L. M. *J. Am. Chem. Soc.* **1982**, *104*, 6825.

(17) Blundell, T. L.; Powell, H. M. *J. Chem. Soc. A* **1971**, 1685.

(18) Arsenault, G. J.; Anderson, C. M.; Puddephatt, R. J. *Organometallics* **1988**, *7*, 2094.

(19) Albinati, A.; Lehner, H.; Venanzi, L. M.; Wolfer, M. *Inorg. Chem.* **1987**, *26*, 3933.

(20) Green, M.; Orpen, A. G.; Salter, I. D.; Stone, F. G. A. *J. Chem. Soc., Dalton Trans.* **1984**, 2497.

(21) Freeman, M. J.; Green, M.; Orpen, A. G.; Salter, I. D.; Stone, F. G. A. *J. Chem. Soc., Chem. Commun.* **1983**, 1332.

(22) Cotton, F. A.; Falvello, L. R.; Uson, R.; Fornies, J.; Tomas, M.; Casas, J. M.; Ara, I. *Inorg. Chem.* **1987**, *26*, 1366.

(23) Sykes, A. G.; Mann, K. R. *Inorg. Chem.*, in press.

(24) Smith, T. P. Ph.D. Thesis, California Institute of Technology, 1982.

0002-7863/90/1512-7247$02.50/0 © 1990 American Chemical Society

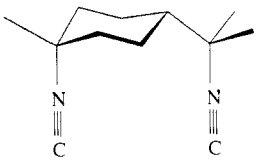

Figure 1. Representation of the 1,8-diisocyano-*p*-menthane ligand.

phosphate[25] salts. All elemental analyses were conducted by MHW Laboratories of Phoenix, AZ.

Synthesis of Starting Materials. (a) $[Ag(PPh_3)_2]PF_6$ and $[Ag(PPh_3)_2]SbF_6$.[26] A 0.295-g sample of $AgPF_6$ (1.2 mmol) was dissolved in 8 mL of acetonitrile. The solution of 0.6113 g of triphenylphosphine (2.4 mmol, 2 equiv) in 10 mL of acetonitrile was added slowly to the Ag^+ solution. After all of the PPh_3 was added and the solution was stirred for 1 h, a small amount of a fine, white precipitate was removed by filtration and discarded. The filtrate was concentrated under vacuum and two additions of ether induced the crystallization of the product in 70% yield. $[Ag(PPh_3)_2](PF_6)$ is a white solid that is stable when kept in the freezer in the dark: $^{31}P\{^1H\}$ NMR (121.5 MH, CH_3CN, 25 °C) 10.8 ppm (s) vs external H_3PO_4. Anal. Calcd $AgC_{36}H_{30}F_6P_3$: C, 55.61; H, 3.89. Found: C, 55.42; H, 3.87.

The synthesis of $[Ag(PPh_3)_2](SbF_6)$ was identical in all respects except $AgSbF_6$ was substituted for $AgPF_6$. The yield in this case was 88%: $^{31}P\{^1H\}$ NMR (121.5 MHz, acetone, 25 °C) 13.8 ppm (s) vs external H_3PO_4. Anal. Calcd for $AgC_{36}H_{30}P_3Sb$: C, 49.78; H, 3.48. Found C, 50.57; H, 4.04.

(b) $[Au(PPh_3)_2](PF_6)$.[27] A 500-mg sample of $Au(PPh_3)Cl$ (1 mmol) was dissolved in 10 mL of distilled CH_2Cl_2. To this solution was added slowly, 420 mg of crushed $AgNO_3$ (2.5 mmol) in 15 mL of methanol. Solid AgCl immediately precipitated and was removed by filtration. The resulting solution was rotovapped to dryness and extracted with 10 mL of CH_2Cl_2. A second filtration followed by rotory evaporation to dryness produced solid $Au(PPh_3)NO_3$ in quantitative yield. A 0.3006-g sample of $Au(PPh_3)NO_3$ (0.58 mmol) was dissolved in 15 mL of distilled CH_2Cl_2. Solid triphenylphosphine (0.1504 g, of 0.58 mmol, 1 equiv) was added to the solution. The solid obtained from rotary evaporation was redissolved in 5 mL of methanol. When 0.2387 g of NH_4PF_6 (1.5 mmol, 2.5 equiv) was added to the methanol solution, a white solid immediately precipitated. The product was collected on a fine frit filter and washed with successive amounts of methanol and pentane. White $[Au(PPh_3)_2](PF_6)$ was produced in 85% yield based on $Au(PPh_3)NO_3$: $^{31}P\{^1H\}$ NMR (121.5 MHz, CH_2Cl_2, 25 °C) 45.4 (s) ppm vs external H_3PO_4. Anal. Calcd for $AuC_{36}H_{30}F_6P_3$: C, 49.90; H, 3.49. Found: C, 49.77; H, 3.48.

Synthesis of Adducts. (a) $[Ir_2(dimen)_4](PPh_3)Au(PPh_3)](PF_6)_3$. A 0.0332-g sample of $[Ir_2(dimen)_4](PF_6)_2$ (0.023 mmol) was dissolved in 10 mL of acetone. When 0.0202 g of $[Au(PPh_3)_2](PF_6)$ (0.023 mmol, 1 equiv) was added, the purple solution slowly bleached to a deep yellow color. The resulting solution was rotovapped to concentrate the solution and then a large excess (~25 mL) of pentane was added to precipitate the complex in quantitative yield: ^1H NMR (200 MHz, CD_2Cl_2, 25 °C) phenyl 7.308–7.806 ppm (m, 30 H); dimen methyl, methylene, and methine protons are observed as multiplets between 2.130 and 1.065 ppm (72 H). Integration confirmed the number of protons in each observed resonance. $^{13}C\{^1H\}$ NMR (50.3 MHz, CD_2Cl_2, 25 °C) phenyl carbons are multiplets centered at 134.05, 133.04, and 130.06 ppm; dimen C-1 (64.91, t), C-2,6 (36.56, d), C-3,5 (22.30, d), C-4 (40.43, d), C-7 (27.50, m), C-8 (69.44, t), C-9,10 (26.72, m); isocyanide carbons not observed. Assignment of signals based on (*Z*)-1,8-diamino-*p*-menthane:[28] IR (acetone) $\bar{\nu}$(CN) 2172, 2150 cm^{-1}; UV/vis (CH_3CN) λ_{max} = 380 nm; $^{31}P\{^1H\}$ NMR (121.5 MHz, CH_2Cl_2, 25 °C) Au–P 41.2 (m), Ir–P –33.2 ppm (m) vs external H_3PO_4; FAB mass spectroscopy *m/e* for $\{[Ir_2(dimen)_4(PPh_3)Au(PPh_3)](PF_6)_2\}^{1+}$ calcd 2157.59, found 2157.4. Theoretical and experimental isotopic intensities and distribution are in close agreement. Anal. Calcd for $AuIr_2C_{84}H_{102}D_{18}N_8P_5$: C, 43.82; H, 4.47; N, 4.97. Found C, 44.02; H, 4.62; N, 5.06.

(b) $[Ir_2(dimen)_4(PPh_3)Ag(PPh_3)](PF_6)_3$. The synthesis of the $Ag(PPh_3)_2^+$ adduct is identical with that of the gold analogue. However, the complex is less stable in solution. Over a period of hours, silver metal precipitates from solutions of the compound. Rapid handling of solutions of the compound is required and the solid was stored under refrigeration: IR (acetone) $\bar{\nu}$(CN) 2168, 2136 cm^{-1}; UV/vis (CH33CN) λ_{max} = 400 nm; $^{31}P\{^1H\}$ NMR (121.5 MHz, CD_3CN, –40 °C, SbF_6^- salt) Ag–P 12 (m), Ir–P –36.2 ppm (m) vs external H_3PO_4. Anal. Calcd for $AgIr_2C_{84}H_{102}F_{18}N_8P_5$: C, 45.59; H, 4.65; N, 5.06. Found: C, 45.33; H, 4.68; N, 5.18.

Table I. Crystallographic Data and Collection Parameters for $[Ir_2(dimen)_4(PPh_3)Au(PPh_3)](PF_6)_3 \cdot CH_3CN$

formula	$AuIr_2C_{86}H_{105}F_{18}N_9P_5$
MW	2302.03
crystal system	monoclinic
space group	*Cc* (No. 9)
cell constants	
a, Å	24.79 (2)
b, Å	15.792 (6)
c, Å	23.307 (6)
α, deg	90
β, deg	94.15 (4)
γ, deg	90
cell vol, $Å^3$	9102
Z	4
d_{calc}, g cm^{-3}	1.680
crystal dimensions, mm	0.45 × 0.35 × 0.25
absorp coeff, cm^{-1}	46.77
intensity data measmnt	–91 °C
diffractometer	Enraf-Nonius CAD4
radiation	Mo Kα (λ = 0.71069 Å) graphite monochromatized
scan type	ω
$2\theta_{max}$, deg	54.1
no. of total reflctns	10086
reflctns with $I * 3.33\sigma(I)$	6382
no. ov variables	431
p	0.05
SD observn of unit weight (GOF)	1.34
R	0.055
R_w	0.064

Instrumentation. Fast atom bombardment mass spectra (FAB-MS) were obtained on a VG Analytical VG 7070E-HF high-resolution double-focusing mass spectrometer equipped with a VG 11/250 data system. Spectra were obtained at a resolution of 1 part in 2000. Ions were generated by bombardment of the target matrix with a neutral Xenon atom beam (derived from a Xe^+ ion beam accelerated at 8 KV). Samples for FAB-MS were prepared by dissolving the complexes in a *m*-nitrobenzoic acid matrix. Simulations of the isotopic distribution patterns were carried out with a program provided with the VG 7070E-HF instrument.

IR spectra were obtained on a Perkin-Elmer 1710 infrared FT spectrometer, and UV–vis spectra were obtained on a Cary 17-D spectrophotometer interfaced to a Zenith 150 microcomputer.

An IBM AC-200 spectrometer was used for ^1H and ^{13}C NMR. Chemical shifts were referenced to the residual proton or carbon resonances of the solvent. All chemical shifts are reported in units of δ. ^{31}P spectra were recorded at 121.5 MHz on a Nicolet NT-300WB spectrometer, and the chemical shifts were referenced to external phosphoric acid run immediately before the samples. NMR simulations were conducted on a Zenith 150 microcomputer using the RACCOON program.[29]

^{31}P–^{31}P δ/J-Resolved NMR Spectroscopy. FIDs were collected by using the pulse sequence $90°-\tau_1-180°-\tau_1$-echo (t_2),[30] with the evolution time t_1 considered as $2\tau_1$ (i.e., the time between the onset of the 90° pulse and the acquisition), ranging incrementally in our case from 5 to 640 ms. Fourier transformation in both time domains (t_2 is the elapsed time of recording the FID) gives a two-dimensional spectrum with two frequency dimensions, f_1 and f_2. Fourier transformation with respect to f_2 gives chemical shift and coupling information. Because t_1 causes modulation in the FID due to P–P coupling constants, f_1 yields the values of coupling constants only, with the splitting pattern centered at zero. Homonuclear two-dimensional δ/J-resolved spectroscopy does not separate chemical shift and coupling constants on the f_2 axis, but a 45° tilting of f_2 subtracts the P–P coupling contributions; thus, after 45° tilting, the two-dimensional series of spectra represent a plot of $^{31}P\{^1H, ^{31}P–^{31}P\}$ decoupled, chemical shifts (f_2) vs P–P couplings (f_1). Resolution in the two-dimensional spectrum is 2.7 Hz/pt in the f_2 dimension and 1.56 Hz/pt in the f_1 dimension, resulting in an approximate ±5 Hz error in the chemical shift and coupling data.

X-ray Data Collection. A yellow prismatic crystal of $[Ir_2(dimen)_4(PPh_3)Au(PPh_3)](PF_6)_3 \cdot CH_3CN$ with approximate dimensions of 0.45

(25) Sykes, A.; Mann, K. R. *J. Am. Chem. Soc.* **1988**, *110*, 8252.
(26) Alyea, E. C.; Malito, J.; Nelson, J. H. *Inorg. Chem.* **1987**, *26*, 4294.
(27) Carriedo, G. A.; Howard, J. A. K.; Marsden, K.; Stone, F. G. A.; Woodward, P. *J. Chem. Soc., Dalton Trans.* **1984**, 1589.
(28) Liptak, A.; Kusiak, J. W.; Pitha, J. *J. Med. Chem.* **1985**, *28*, 1699.
(29) Schatz, P. F. RACCOON was written for the IBM microcomputer.
(30) Aue, W. P.; Karhan, J.; Ernst, R. R. *J. Chem. Phys.* **1976**, *64*, 4266.

× 0.35 × 0.25 mm was obtained by the slow diffusion of ether into a concentrated acetonitrile solution containing the complex. X-ray collection and refinement data are summarized in Table I. The crystal belongs in the monoclinic system with four molecules in the unit cell. Cell constants obtained from a least-squares refinement using the setting angles of 25 carefully centered reflections in the range $18.00 < 2\theta < 39.00°$ are $a = 24.79$ (2), $b = 15.792$ (6), $c = 23.307$ (6) Å; $\beta = 94.15$ (4)°. Systematic absences (hkl, $h + k \neq 2n$; $h0l$, $l \neq 2n$) and the successful refinement of the structure identified the space group as Cc (No. 9). FW = 2302.03, and the calculated density is 1.680 g/cm^3. All measurements were made on an Enraf-Nonius CAD-4 diffractometer with graphite monochromated Mo Kα radiation ($\lambda = 0.71069$ Å).

The data were collected at a temperature of −91 ± 1 °C with the ω scan technique to a maximum 2θ value of 54.1°. Of the 10086 reflections collected, 10082 were unique ($R_{int} = 0.231$). The intensities of three representative reflections, which were measured after every 100 min of X-ray exposure time, remained constant throughout data collection, indicating crystal and electronic stability. No decay correction was applied. The linear absorption coefficient for Mo Kα is 46.8 cm^{-1}. An empirical absorption correction, using the program DIFABS,[31] was applied, which resulted in transmission factors ranging from 0.8 to 1.23. The data were corrected for Lorentz and polarization effects.

Structure Solution and Refinement. The structure was solved by direct methods.[32] Two of the PF_6^- anions and one dimen ligand (labeled J) are disordered. This dimen ligand was disordered end for end as has been previously observed.[25] This disorder resulted in 100% occupancy factors for the atoms with common positions (C1, N1, C2, C′, N′, C2′, C4, and C6) and 50% occupancy factors for C3, C5, C7, C8, C9, and C10. All were refined isotropically. The phenyl rings of the PPh_3 ligands were included as rigid groups in the refinement. The non-hydrogen atoms were refined anisotropically. Hydrogen atoms were included in the structure factor calculation in idealized positions ($d_{C-H} = 0.95$ Å) and were assigned isotropic thermal parameters that were 20% greater than the $B_{equivalent}$ value of the atom to which they were bonded. The final cycle of full-matrix least-squares refinement,[33] based on 6382 observed reflections [$I > 3.00\sigma(I)$] and 431 variable parameters, converged (largest parameter shift was 0.06 times its esd) with unweighted and weighted agreement factors of $R = \sum||F_o| - |F_c||/\sum|F_o| = 0.055$, and $R_w = [(\sum w(|F_o| - |F_c|)^2/\sum wF_o^2)]^{1/2} = 0.064$. The standard deviation of an observation of unit weight[34] was 1.34. The weighting scheme was based on counting statistics and included a factor ($p = 0.05$) to downweight the intense reflections. The maximum and minimum peaks on the final difference Fourier map corresponded to 1.91 and −1.50 e$^-$/Å^3, respectively.

Neutral atom scattering factors were taken from Cromer and Waber.[35] Anomalous dispersion effects were included in F_{calc};[36] the values for $\Delta f'$ and $\Delta f''$ were those of Cromer.[37] All calculations were performed with the TEXSAN[38] crystallographic software package of Molecular Structure Corp.

Results and Discussion

The addition of $Ag(PPh_3)_2^+$ or $Au(PPh_3)_2^+$ to a dichloromethane solution of $[Ir_2(dimen)_4]^{2+}$ in a 1:1 ratio immediately affords the yellow complexes **1** and **2** according to eq 1. Addition

$$[M(PPh_3)_2](PF_6) + [Ir_2(dimen)_4](PF_6)_2 \rightarrow [Ir_2(dimen)_4(PPh_3)M(PPh_3)](PF_6)_3 \quad (1)$$

M = Ag (**1**), Au (**2**)

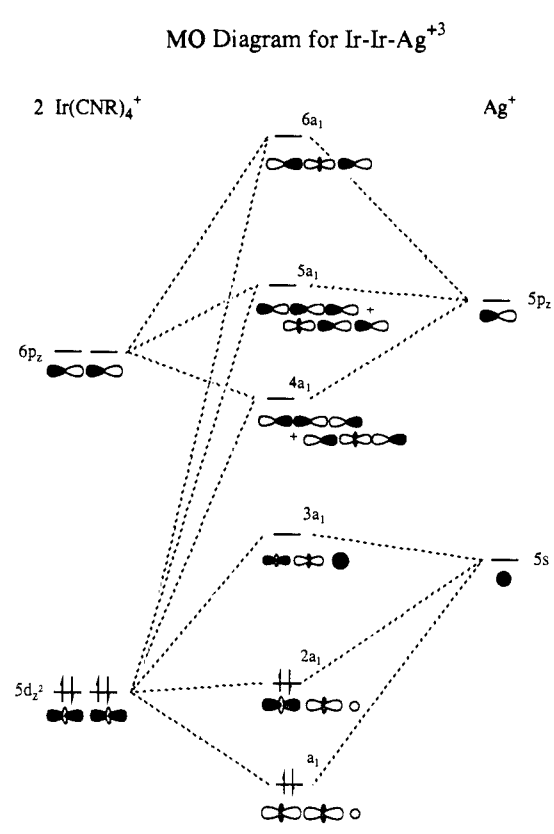

Figure 2. Qualitative molecular orbital diagram for $[Ir_2(dimen)_4(PPh_3)M(PPh_3)]^{3+}$ (M = Ag, Au) illustrating the metal–metal bonding within the Ir–Ir–M core.

of pentane to the dichloromethane solutions produces dark yellow solids in nearly quantitative yields. The Au complex is air and light stable for an indefinite time in solution, while the Ag complex is oxidized over a period of hours, particularly in nonpolar solvents such as dichloromethane. The products of these oxidation reactions will be the subject of a future report. Compounds **1** and **2** are formulated as end-bound adducts of the $M(PPh_3)^+$ unit, with the second PPh_3 group bound at the opposite Ir(I) center, on the basis of spectroscopic and X-ray diffraction data (vide infra).

The infrared spectral properties of complexes **1** and **2** are consistent with the formation of a donor–acceptor bond between $M(PPh_3)^+$ and $[Ir(dimen)_4]^{2+}$. Both complexes exhibit two isocyanide stretching frequencies [(**1**) 2168, 2136 cm^{-1}; (**2**) 2172, 2150 cm^{-1}] in CH_2Cl_2 solution, which suggest that the two iridium metal centers of the binuclear $[Ir_2(dimen)_4]^{2+}$ unit are not equivalent. As previously reported, the value of the $\bar{\nu}$(CN) stretching frequency of isocyanide complexes is a good, qualitative measure of the relative oxidation level of the metal center.[39] Thus, the infrared stretching frequency of the parent $Ir_2(dimen)_4^{2+}$ (2155 cm^{-1}) is about midway between the two stretching frequencies exhibited by each of the new compounds. The shift of one of the IR bands to higher energy and the other to lower energy indicates the binding of the Lewis acid $M(PPh_3)^+$ unit decreases the electron density at one of the iridium atoms while the coordination of PPh_3 to the opposing iridium atom increases the electron density.

A qualitative molecular orbital diagram that illustrates the σ bonding within the Ir–Ir–M (M = Ag, Au) unit is shown in Figure 2. Significant σ-bonding M–Ir interactions occur in the two lowest filled molecular orbitals. The 25 000- and 26 300-cm^{-1} absorptions in **1** and **2**, respectively, are assigned to the $2a_1 \rightarrow 3a_1$ transition. Of interest, the analogous transition in the encapsulated $[AgIr_2(dimen)_4]^{2+}$ ($a_{2u} \rightarrow 2a_{1g}$) is at considerably higher energy. The net metal–metal bonding (two M–Ir bonds) in the encapsulated adduct is stronger than that of the "outside" adducts with a M–Ir and a weaker Ir–Ir interaction.

(31) DIFABS: Walker, S. *Acta. Crystallogr.* **1983**, *A39*, 158.
(32) Structure Solution Methods: Gilmore, C. J. MITHRIL—an integrated direct methods computer program. *J. Appl. Crystallogr.* **1984**, *17*, 42. Beurskens, P. T. DIRDIF—direct methods for difference structures—an automatic procedure for phase extension and refinement of difference structure factors. Technical Report 1984/1; Crystallography Laboratory, Toernooiveld, 6525 Ed Nijmegen, Netherlands.
(33) Least squares: function minimized $\sum w(|F_o| - |F_c|)^2$, where $w = 4F_o^2/\sigma^2(F_o^2)$ and $\sigma^2(F_o^2) = [S^2(C + R^2B) + (pF_o^2)^2]/Lp^2$. S is the scan rate, C is the total integrated peak count, R is the ratio of scan time to background counting time, B is the total background count, Lp is the Lorentz-polarization factor, and p is the p factor.
(34) Standard deviation of an observation of unit weight: $[\sum w(|F_o| - |F_c|)^2/(NO - NV)]^{1/2}$; where NO is the number of observations and NV is the number of variables.
(35) Cromer, D. T.; Waber, J. T. In *International Tables for X-ray Crystallography*; Kynoch Press: Birmingham, England, 1974; Vol. IV, Table 2.2 A.
(36) Ibers, J. A.; Hamilton, W. C. *Acta Crystallogr.* **1964**, *17*, 781.
(37) Cromer, D. T. In *International Tables for X-ray Crystallography*; Kynoch Press: Birmingham, England, 1974; Vol. IV, Table 2.3.1.
(38) TEXSAN—TEXRAY Structure Analysis Package, Molecular Structure Corp., 1985.
(39) Mann, K. R.; DiPierro, M.; Gill, T. P. *J. Am. Chem. Soc.* **1980**, *102*, 3965.

Table II. Selected Distances Involving the Nonhydrogen Atoms[a]

atom	atom	distance	ADC(*)	atom	atom	distance	ADC(*)
AU1	P2	2.199 (7)	1	C5G	C6G	1.58 (4)	1
AU1	IR2	2.607 (2)	1	C6G	C7G	1.41 (6)	1
IR1	C1H′	1.89 (2)	1	C9G	C2G′	1.49 (5)	1
IR1	C1I′	1.94 (2)	1	C10G	C2G′	1.41 (6)	1
IR1	C1G	2.01 (2)	1	C1G′	N1G′	1.21 (3)	1
IR1	C1J	2.06 (2)	1	N1G′	C2G′	1.50 (4)	1
IR1	P1	2.482 (7)	1	C1H	N1H	1.17 (3)	1
IR1	IR2	2.986 (2)	1	N1H	C2H	1.49 (3)	1
IR2	C1H	1.90 (2)	1	C2H	C3H	1.48 (4)	1
IR2	C1I	1.93 (2)	1	C2H	C8H	1.51 (4)	1
IR2	C1G′	1.97 (2)	1	C2H	C7H	1.53 (4)	1
IR2	C1J′	2.01 (2)	1	C3H	C4H	1.48 (4)	1
P1	C1C	1.82 (1)	1	C4H	C5H	1.60 (4)	1
P1	C1B	1.82 (1)	1	C5H	C6H	1.50 (4)	1
P1	C1A	1.85 (1)	1	C5H	C2H′	1.58 (4)	1
P2	C1E	1.79 (2)	1	C6H	C7H	1.47 (4)	1
P2	C1D	1.81 (2)	1	C9H	C2H′	1.47 (4)	1
P2	C1F	1.82 (2)	2	C10H	C2H′	1.51 (4)	1
C1G	N1G	1.15 (3)	1	C1H′	N1H′	1.16 (3)	1
N1G	C2G	1.45 (3)	1	N1H′	C2H′	1.51 (3)	1
C2G	C3G	1.54 (4)	1	C1I	N1I	1.12 (3)	1
C2G	C8G	1.61 (6)	1	N1I	C2I	1.45 (3)	1
C2G	C7G	1.67 (6)	1	C2I	C8I	1.45 (5)	1
C3G	C4G	1.57 (4)	1	C2I	C3I	1.55 (4)	1
C4G	C5G	1.40 (4)	1	C2I	C7I	1.56 (4)	1
C5G	C2G′	1.56 (4)	1	C3I	C4I	1.51 (5)	1
C4I	C5I	1.62 (4)	1	C5J	C7J′	1.85 (7)	1
C5I	C6I	1.51 (5)	1	C6J	C5J′	1.52 (7)	1
C5I	C2I′	1.56 (4)	1	C6J	C7J′	1.60 (6)	1
C6I	C7I	1.48 (5)	1	C6J	C7J	1.66 (5)	1
C9I	C2I′	1.44 (4)	1	C7J	C5J′	1.52 (8)	1
C10I	C2I′	1.57 (4)	1	C7J	C10J′	1.69 (8)	1
C1I′	N1I′	1.14 (3)	1	C8J	C10J′	1.2 (1)	1
N1I′	C2I′	1.46 (3)	1	C8J	C9J′	1.68 (9)	1
C1J	N1J	1.13 (3)	1	C9J	C3J′	1.2 (1)	1
N1J	C2J	1.48 (4)	1	C9J	C2J′	1.73 (7)	1
C2J	C7J	1.45 (5)	1	C10J	C8J′	1.03 (8)	1
C2J	C9J′	1.46 (7)	1	C10J	C2J′	1.35 (6)	1
C2J	C8J	1.52 (7)	1	C10J	C7J′	1.45 (7)	1
C2J	C3J	1.53 (8)	1	C1J′	N1J′	1.11 (3)	1
C2J	C10J′	1.56 (8)	1	N1J′	C2J′	1.55 (4)	1
C2J	C5J′	1.74 (8)	1	C2J′	C3J′	1.47 (9)	1
C3J	C9J′	1.2 (1)	1	C2J′	C8J′	1.64 (8)	1
C3J	C5J′	1.6 (1)	1	C2J′	C7J′	1.71 (7)	1
C3J	C4J	1.61 (8)	1				
C4J	C5J	1.46 (6)	1				
C4J	C5J′	1.48 (7)	1				
C4J	C3J′	1.66 (9)	1				
C5J	C5J′	1.34 (8)	1				
C5J	C3J′	1.36 (9)	1				
C5J	C2J′	1.55 (6)	1				
C5J	C6J	1.60 (5)	1				

[a] Distances are in angstroms. Estimated standard deviations in the least significant figure are given in parentheses.

Crystallography of $[Ir_2(dimen)_4(PPh_3)Au(PPh_3)](PF_6)_3 \cdot CH_3CN$. The structure of complex **2** was determined by single-crystal X-ray diffraction methods. The compound contains a two-centered two-electron Ir–Au(PPh_3) bond plus several other interesting features. The crystallographic information is summarized in Table I and selected bond distances are given in Table II.

A formula unit within the crystal structure consists of a tripositive cation, three PF_6^- anions (two of which are rotationally disordered about the central phosphorus atom), and an interstitial acetonitrile molecule. The cation consists of two Ir atoms in pseudooctahedral configurations with the two axial positions of the parent $[Ir_2(dimen)_4]^{2+}$ complex occupied by a $Au(PPh_3)^+$ group and a triphenylphosphine ligand. Figure 3 shows a labeled ORTEP drawing of the cation.

The structure revealed one of the four dimen ligands was disordered in a 50/50 "head-to-tail" arrangement that is typical of complexes containing the unsymmetrical dimen group.[23,25,40-42] More surprisingly, based on previous results, the three other dimen ligands are ordered and are arranged with two of the cis ligands positioned with the dimethyl-substituted and directed toward the $Au(PPh_3)^+$ group (see Figure 1 for a representation of the dimen ligand). The third ordered dimen ligand is positioned with the dimethyl-substituted end directed in the Ir–PPh_3 direction. Because the fourth disordered dimen ligand does not show any end-to-end site preference, the crystal consists of a 50/50 mixture of the 2:2 cis (A) and the 3:1 (C2) isomers (vide infra, Figure 4). It is interesting that these two isomers present in the crystal represent half of the total statistical mix of isomers possible. Apparently, crystal-packing forces are similar enough for these

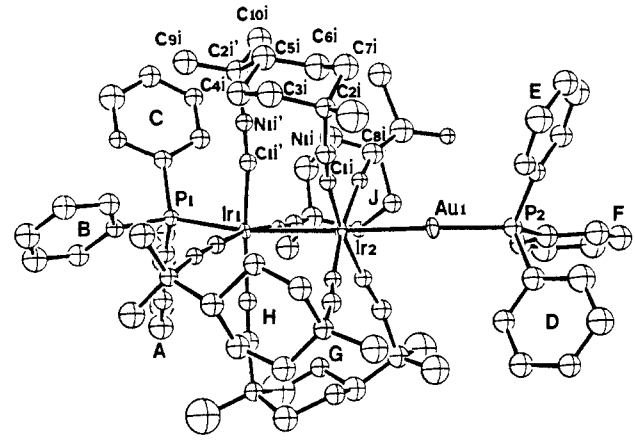

Figure 3. ORTEP drawing of the $[Ir_2(dimen)_4(PPh_3)Au(PPh_3)]^{3+}$ cation that illustrates the numbering scheme. Triphenylphosphine rings are labeled with the suffixes A–F. The dimen ligands are indicated with suffixes G–J.

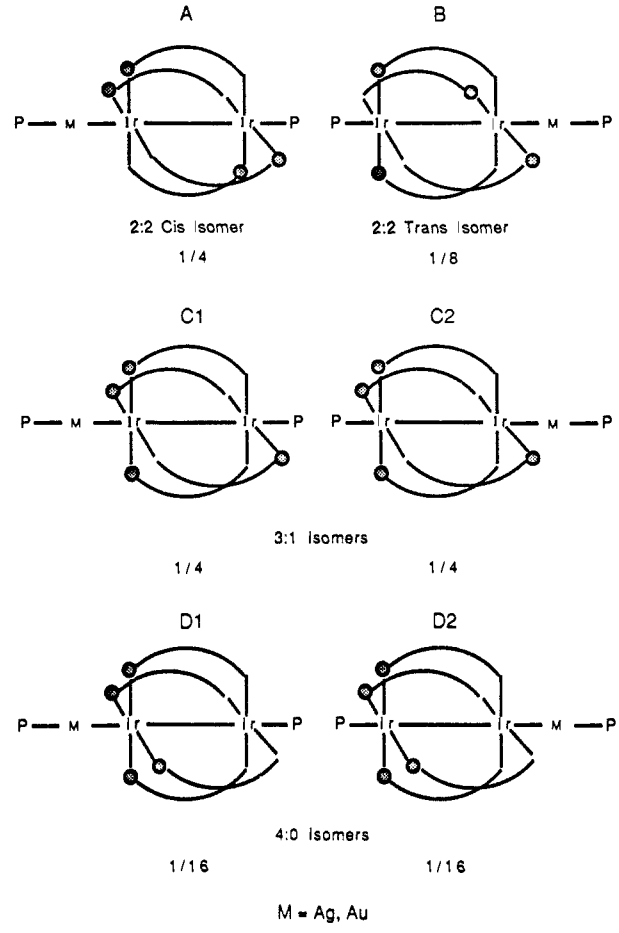

Figure 4. Schematic representations of the six possible geometric isomers of $[Ir_2(dimen)_4(PPh_3)M(PPh_3)]^{3+}$ due to the axial binding of the M(PPh_3) and PPh_3 groups and the head-to-tail distributions of the four unsymmetrical 1,8-diisocyanide-*p*-menthane ligands. The fraction indicates the statistical amount expected for each isomer.

(40) Che, C.-M.; Herbstein, F. H.; Schaefer, W. P.; Marsh, R. E.; Gray, H. B. *Inorg. Chem.* **1984**, *23*, 2572.
(41) Mann, K. R. *Cryst. Struct. Commun.* **1981**, *10*, 451.
(42) Gladfelter, W. L.; Gray, H. B. *J. Am. Chem. Soc.* **1980**, *102*, 5909.

two isomers to crystallize together with the exclusion of the other four isomers. These structural results demonstrate that the sterically more demanding PPh_3 [vs the $Au(PPh_3)^+$ group] can occupy the more sterically congested end of the 3:1 isomer (C2). ^{31}P NMR solution studies showing that most of the possible isomers are initially present in bulk samples of the complex are discussed below. An attempt (^{31}P NMR) to show the depletion of the particular isomers in the mother liquor that produced the crystals used in the X-ray structure determination was unsuccessful because of low concentration.

The four bridging dimen ligands are coordinated to the two Ir atoms in nearly regular square-planar configurations. The angles between cis ligands around the Ir centers range from 84.7 (9)° to 94.1 (8)° around Ir1 and from 87.8 (9)° to 91 (1)° around Ir2. The angles between trans isocyanide ligands are 170.9 (8)° and 176 (1)° for Ir1 and are identical within experimental error with those for Ir2 [172 (1)° and 173 (1)°]. The Ir–C bond lengths [1.89 (2) to 2.06 (2) Å around Ir1 and 1.90 (2) to 2.01 (2) Å around Ir2] are reasonable distances for square-planar Ir isocyanide complexes.[24]

The Ir2–Au vector is nearly orthogonal to the $Ir2(CNR)_4$ square plane [average C–Ir2–Au angle is 86.2 (7)° with minimum and maximum values of 85.0 (7)° and 88.0 (7)°, respectively]. The P1–Ir1 vector is also orthogonal to the $Ir1(CNR)_4$ plane [average C–Ir1–P1 angle is 91.8 (7)° with minimum and maximum values of 86.8 (6)° and 96.6 (7)°, respectively].

The Au–Ir2 bond distance [2.607 (2) Å] is short compared with values in similar compounds (values range from 2.625 to 2.765 Å[9-16]). The shortest previous Ir–Au bond distance (2.625 Å) was found in $[Ir(dppe)_2Au(PPh_3)]^{2+}$, the only other structure that contains the unsupported two-center two-electron $Ir–Au(PPh_3)$ unit.[13] In **2**, no other significant bonding interactions exist between the Au and neighboring atoms except for the terminal triphenylphosphine ligand. The measured Au–P2 distance [2.199 (7) Å] is also slightly shorter than the values found in other Ir–Au phosphine complexes (values range from 2.219 to 2.290 Å).[9-16] Also of significance, the Ir1–P1 bond distance [2.482 (7) Å] is significantly longer than Ir–P distances previously determined (values range from 2.27 to 2.357 Å).[9-16]

The bonding along the axial direction in **2** is consistent with a strong donor–acceptor $Ir^+–AuPPh_3^+$ interaction that results in short Ir–Au and Au–P bond distances, typical of two-coordinate gold. At the other end of the $Ir_2(dimen)_4^{2+}$ unit, the triphenylphosphine ligand is bound with a relatively long Ir–P distance. Both electronic and steric considerations are probably important in determining the axial bonding in **2**. For example, the longer Ir–Au and Au–P bond distances found in $[Ir)dppe)_2Au(PPh_3)]^{2+}$ may in part be due to steric crowding of the phenyl rings of the $Au(PPh_3)^+$ unit with the phenyl rings on the chelating dppe basal plane ligands. The dimen ligand in **2** is less congested near the Ir atoms because the methyl groups on the quaternary carbons are at a greater distance from the Ir metal centers. The opposite is true for the triphenylphosphine directly bonded to the Ir in **2**.

An unexpected feature found in the X-ray structure of **2** is the relatively short Ir–Ir bond distance [2.986 (2) Å]. Although the Ir–Ir bond distance in $[Ir_2(dimen)_4]^{2+}$ has not been measured, the X-ray structure of the analogous $[Rh_2(dimen)_4]^{2+}$ complex reveals an internuclear Rh–Rh separation of 4.479 (2) Å.[41] Typically, the large metal–metal distances of the d^8–d^8 complexes are drastically reduced when halogens (i.e., Cl_2) are transannually added across the two d^8 metal centers to yield binuclear d^7–d^7 complexes with formal M–M bond orders of 1. M–M values of 2.77 and 2.80 Å have previously been determined for X–M–M–X^{2+} species.[43,24] The 2.986 (2) Å Ir–Ir distance in **2** is intermediate in value between typical d^8–d^8 and d^7–d^7 binuclear complexes and confirms that the Lewis acid character of the $Au(PPh_3)^+$ acceptor moiety is transmitted through Ir2 to also involve Ir1.

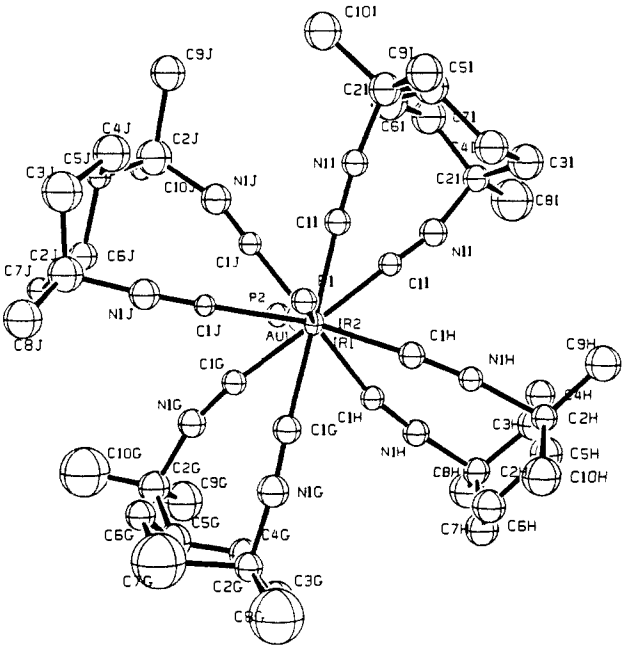

Figure 5. ORTEP drawing of the $[Ir_2(dimen)_4(PPh_3)Au(PPh_3)]^{3+}$ cation viewed down the Ir1–Ir2 bond axis. The twist angle of the $Ir(CNR)_4$ planes is 39°. The phenyl rings of the triphenylphosphine ligands have been omitted.

Another interesting feature of this structure is the significant torsional angle between the two $Ir(CNR)_4$ square planes that accompany the shortening of the Ir–Ir distance. Figure 5 shows an ORTEP drawing of **2** viewed directly down the Ir–Ir axis with the phenyl rings of the two triphenylphosphine ligands omitted. This drawing clearly shows that the $Ir(CNR)_4$ square planes have adopted a nearly staggered configuration to accommodate the shortened Ir1–Ir2 distance. The average C#1–Ir1–Ir2–C#1′ torsional angle (# = G, H, I, or J designation for the respective dimen ligands) is 39 (1)° with minimum and maximum values of 34 (1)° and 42.4 (8)°, respectively. The 39° staggering of the $Ir(CNR)_4$ planes is larger than the 31° twisting found in $Rh_2(TM4)_4Cl_2^{2+}$[43] and $Ir_2(TM4)_4I_2^{2+}$[24] (TM4 = 2,5-dimethyl-2,5-diisocyanohexane). To accommodate the significant shortening of the M–M distance, the dimen ligands, with a larger, preferred bridging distance than the TM4 ligand in the M(I) compounds, require a greater staggering of the $Ir(CNR)_4$ planes to achieve the smaller Ir–Ir spacing in the adduct. The dimen ligand accommodates a remarkable variation in bridging distances, which range from 5.28 Å in the encapsulated $[AgIr_2(dimen)_4(PPh_3)_2]^{3+}$[23] to 3.16 Å in $[Rh_2(dimen)_2(dppm)_2]^{2+}$ and 2.986 (2) Å in **1**.[44] Also apparent from Figure 5 is the slight bowing of the P–Ir–Ir–Au–P^{3+} core [P1–Ir1–Ir2 is 170.2 (1)°; Ir1–Ir2–Au is 172.86 (5)°; and Ir2–Au–P2 is 174.2 (2)°]. The deviation from linearity is likely due to steric interactions between the PPh_3 phenyl rings and the dimen methyl groups.

The least-squares planes defined by the atoms C1G–C1H′–C1I′–C1J and C1G′–C1H–C1I–C1J′ (C1G–J are the isocyanide carbon atoms) relate the positions of the Ir1 and Ir2 metal centers, respectively, to the two $Ir(CNR)_4$ coordination spheres. The displacement of Ir1 from the least-squares plane defined as C1G–C1H′–C1I′–C1J is 0.06 Å toward the triphenylphosphine bound to it in the axial Ir_2^{2+} site. The displacement of Ir2 from the least-squares plane defined as C1G′–C1H–C1I–C1J′ is 0.13 Å away from the $Au(PPh_3)^+$ unit and toward Ir1. These small out-of-plane deviations of the iridium atoms indicate that the isocyanide carbons of the dimen ligands supply nearly planar-equatorial coordination at both iridium metal centers with a slight shift away from the sterically more demanding triphenylphosphine ligand affixed to Ir1.

(43) Maverick, A. W. Ph.D. Thesis, California Institute of Technology, 1982. MIskowski, V. M.; Smith, T. P.; Lochr, R. M.; Gray, H. B. *J. Am. Chem. Soc.* **1985**, *167*, 7925.

(44) Boyd, D. C.; Matsch, P. A.; Mixa, M. M.; Mann, K. R. *Inorg. Chem.* **1986**, *25*, 3331.

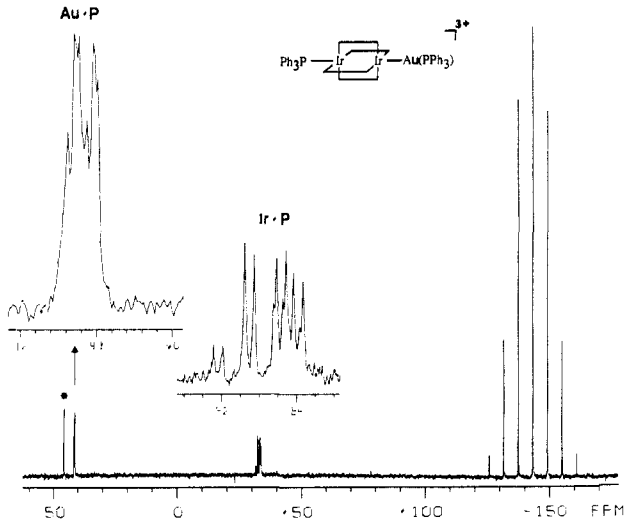

Figure 6. One-dimensional 121.5-MHz $^{31}P\{^1H\}$ spectrum of $[Ir_2(dimen)_4(PPh_3)Au(PPh_3)](PF_6)_3$ in CH_2Cl_2 at 25 °C. The asterisk marks the signal due to excess $[Au(PPh_3)_2](PF_6)$.

$^{31}P\{^1H\}$ NMR Solution Studies. (a) Assignment of the ^{31}P NMR Spectrum of 2. In another report,[23] the X-ray crystal structure of $[AgIr_2(dimen)_4(PPh_3)_2](PF_6)_3$ indicated that the unsymmetrical dimen ligands were highly disorderd in a head-to-tail manner, but it was not possible to determine from the X-ray data whether all the possible isomers were present in the solid, or if a single, but crystallographically disordered isomer was present. $^{31}P\{^1H\}$ NMR solution studies confirmed that a statistical distribution of four geometric isomers with different head-to-tail orientations of the unsymmetrical dimen ligands occurred in the bulk sample of the complex. The determination that, at most, only two of the possible isomers are present in the single-crystal X-ray structure of $[Ir_2(dimen)_4(PPh_3)Au(PPh_3)](PF_6)_3$ **2** indicates that multiple isomeric forms exist for this compound as well. As in the previous case, the X-ray structure result does not necessarily prove that the bulk sample and crystals contain the same number or relative amounts of individual isomers. In this case, binding a triphenylphosphine and a $M(PPh_3)^+$ (M = Ag, Au) ligand simultaneously to the ends of the $Ir_2(dimen)_4^{2+}$ parent complex in **1** and **2** results in lowered symmetry for the outside adducts and consequently increases the number of potential isomers. Examination of the one-dimensional $^{31}P\{^1H\}$ spectrum of **2** reveals that many isomers with their characteristic chemical shifts and coupling constants are present. As in the previous case of the encapsulated $[AgIr_2(dimen)_4(PPh_3)_2]^{3+}$, the complexity of the one-dimensional $^{31}P\{^1H\}$ spectrum required the use of two-dimensional techniques to resolve the specific pattern of isomers.[23,45-48]

The one-dimensional $^{31}P\{^1H\}$ NMR spectrum of **2** reveals the PF_6^- septet at −144 ppm and two complex multiplets for the coordinated Ir–Au(PPh_3) and Ir–PPh_3 phosphorus-containing groups at 41.2 and −33.2 ppm, respectively (Figure 6). Integration of the two multiplets confirms they are present in a 1:1 ratio. The peak at 45.4 ppm (marked by an asterisk) is due to a small excess of $[Au(PPh33)_2](PF_6)$. The complexity of the two PPh_3 multiplets arises from the mixture of geometric isomers produced when the iridium binuclear parent complex $[Ir_2(dimen)_4](PF_6)_2$ is synthesized. Formation of the outside Ag and Au adducts increases the theoretical number of isomers from four in the encapsulated $[AgIr_2(dimen)_4(PPh_3)_2]^{3+}$ complex[23] to six. The six possible isomers are schematically represented in Figure 4. The solid circle of the schematically depicted dimen ligand represents the dimethyl-substituted quaternary end of the diisocyanide ligand. Six configurations are possible because the $M(PPh_3)^+$ and PPh_3 units may bind at either end of the unsymmetric 3:1 and 4:0 $[Ir_2(dimen)_4]^{2+}$ isomers. The 2:2 cis and 2:2 trans isomers do not exhibit additional isomerism or site preference because both ends of the $[Ir_2(dimen)_4]^{2+}$ unit in these isomers are equivalent. If these six isomers are formed in statistical amounts, A, B, C1, C2, D1, and D2 would be present in relative amounts of 1/8, 1/4, 1/4, 1/4, 1/16, and 1/16, respectively.

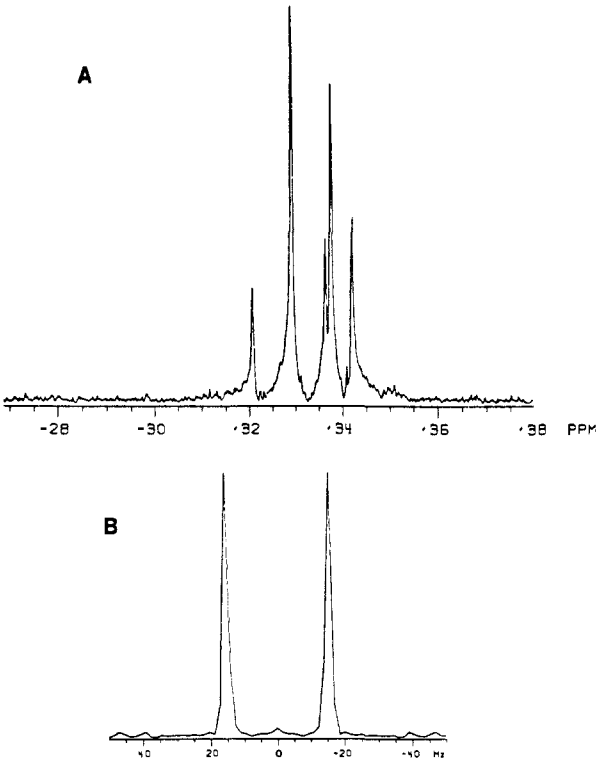

Figure 7. The 45°-tilted, homonuclear δ/J-resolved two-dimensional $^{31}P\{^1H\}$ NMR spectrum of $[Ir_2(dimen)_4(PPh_3)Au(PPh_3)](PF_6)_3$ in CH_2Cl_2 at 25 °C recorded at 121.5 MHz on a Nicolet NT-300WB spectrometer. Spectrum A shows the P–P-decoupled chemical shift information, while spectrum B is along the P–P coupling axis and shows the ca. 3-Hz P–P coupling found for all peaks in A. A data matrix of 128 × 1024 points was acquired in the τ_1, τ_2 domains, and four transients for each value of τ_1 gave a sufficient signal-to-noise ratio.

In **2**, each of the six isomers has an observable P–P coupling because the Au–P and Ir–P environments are chemically nonequivalent for each of the six isomers. If eq 1 produces a statistical number of isomers with no isomeric preference, both Au–P and Ir–P multiplets are the superposition of the signals due to the six isomeric species that exhibit six separate Au–P signals coupled pairwise to six distinct Ir–P signals. The absence of the coupling due to ^{107}Ag and ^{109}Ag nuclei that greatly complicated our analysis of $[AgIr_2(dimen)_4(PPh_3)_2]^{3+}$ enormously simplifies the interpretation of the one-dimensional $^{31}P\{^1H\}$ spectrum of **2**. Without resorting to two-dimensional δ/J-resolved spectroscopic techniques, the Au–P and Ir–P multiplets in Figure 6 appear as a collection of doublets with ~30-Hz coupling constants. Counting the number of doublets in the Ir–P multiplet reveals that at least five and possibly six different doublet resonances exist. This is in rough agreement with the number of isomers predicted. Resolution of the possibility that the shoulder on the most upfield shifted doublet (the signal that would be assigned to the sixth isomer) might actually be noise and the specific assignment of each signal, required the use of two-dimensional δ/J-resolved spectroscopy.

Figure 7 shows the 45°-tilted, 121.5-MHz, homonuclear two-dimensional $^{31}P\{^1H\}$ δ/J-resolved spectrum of the Ir–P multiplet in **2** at −33.2 ppm. The two-dimensional data for the Au–P multiplet at 41.2 ppm were not collected. Figure 7A exhibits the phosphorus-decoupled chemical shift data on the f_2 axis (heteronuclear coupling is absent in this particular case), and Figure

(45) Colquhoun, I. J.; McFarlane, W. *J. Chem. Soc., Chem. Commun.* **1982**, 484.
(46) Chiu, K. W.; Rzepa, H. S.; SHeppard, R. N.; Wilkinson, G.; Wong, W. K. *J. Chem. Soc., Chem. Commun.* **1982**, 482.
(47) Chiu, K. W.; Howard, C. G.; Rzepa, H. S.; Sheppard, R. N.; Wilkinson, G.; Galas, A. M. R.; Hursthouse, M. B. *Polyhedron* **1982**, *1*, 441.
(48) Chiu, K. W.; Rzepa, H. S.; Sheppard, R. N.; Wilkinson, G.; Galas, A. M. R.; Hursthouse, M. B. *Polyhedron* **1982**, *1*, 809.

Table III. ^{31}P NMR Data for $[Ir_2(dimen)_4(PPh_3)M(PPh_3)](PF_6)_3$ (M = Ag, Au)

	$[Ir_2(dimen)_4(PPh_3)AuPPh_3]^{3+}$			$Ir_2(dimen)_4(PPh_3)AgPPh_3]^{3+}$				
	chem shifts, ppm			chem shifts, ppm		coupling const, Hz		
						1-bond[b]	3-bond[c]	
isomer	Au-P[a]	Ir-P	J_{P-P}	Ag-P[a]	Ir-P	J_{Ag-P}	J_{Ag-P}	J_{P-P}
A	41.2	-33.62	30	11.9	-37.63	512 440	31	19
B	41.2	-33.53	30	11.9	-37.63	512 440	31	19
C1	41.2	-32.77	30	11.9	-36.89	512 440	31	19
C2	41.2	-34.06	30	11.9	-38.20	512 440	31	19
D1	41.2	-31.92	30	11.9	-36.21	512 440	31	19
D2								

[a] Values represent an average chemical shift of all the M-P resonances. [b] The upper value is $J_{^{109}Ag-P}$ coupling and the lower value is $J_{^{107}Ag-P}$ coupling. [c] ^{107}Ag and ^{109}Ag couplings were unresolved.

8B is a representative example of the f_1 axis (P-P coupling information) obtained for the peaks found along the f_2 axis. The five peaks found in Figure 7A indicate that only five of the possible six isomers of **2** are present in solution, and that J_{P-P} determined from Figure 8B is on the order of 30 Hz for all the isomers. Figure 7A indicates that the shoulder associated with the upfield doublet in the one-dimensional Ir-P mutliplet (Figure 6) is an artifact due to extraneous noise and is not due to the sixth isomer.

The experimental Ir-P one-dimensional spectrum (Figure 8B) is in close agreement with the simulated $^{31}P\{^1H\}$ spectrum given in Figure 8A. Table III lists the spectral constants used to simulate Figure 8A. Only five of six isomers are simulated with the sterically most crowded 4:0 (D2) isomer omitted. The 30-Hz P-P coupling constant was read directly off the f_1 axis in Figure 8B for all the isomers as an initial starting point for simulating the one-dimensional $^{31}P\{^1H\}$ spectrum and was found to be satisfactory for the final simulation.

In Figure 8A, the peaks labeled A and B represent the 2:2 cis and trans isomers that should be present in the statistical 2:1 ratio and make up 0.375 of the total. Experimentally, the integration of the A and B resonances is 0.357. The peaks labeled C1 and C2 are due to triphenylphosphine binding to unique ends of the 3:1 $[Ir_2(dimen)_4]^{2+}$ complex. In this case the contributions of C1 and C2 are statistically equal to 1/4 each for a total of 1/2. The relative experimental integration of the peaks due to C1 and C2 is 0.279 + 0.259 = 0.538. The slightly larger area of C1 vs C2 indicates the equilibria are shifted in favor of the less hindered C1 isomer. The PPh_3 phenyl rings only interact with one dimethyl-substituted end of a dimen ligand in the C1 isomer vs three dimethyl-substituted ends in C2.

The spectra noticeably lack a second D designated isomer. We suggest that the D2 designated isomer is *not* formed in solution because the attachment of a triphenylphosphine ligand to Ir in D2 requires a less favorable steric interaction between the triphenylphosphine phenyl rings and eight dimen methyl groups. The smallest doublet is then assigned the D1 designation primarily because the triphenylphosphine ligand attached to Ir in D1 involves fewer steric interactions between the three phenyl rings on PPh_3 and only four methyl substitutents on the four dimen ligands. Thus, the formation of the Ir-PPh_3 bond in the 4:0 isomers is limited to the sterically less hindered position in D1, which should be present as 1/8 of the total. The relative experimental integration of the D1 peaks equals 0.106, slightly less than the 1/8 or 0.125 statistical distribution predicted if both the D designated isomers are formed as D1.

The four-bond, 30-Hz P-P coupling found in **2** is higher than the four-bond 21-Hz P-P coupling in the encapsulated Ag compound $[AgIr_2(dimen)_4(PPh_3)_2](PF_6)_3$.[23] The large, through-metal P-Au-Ir-Ir-P phosphorus coupling is likely due to the coordination number of 2 for Au^+ (sp hydridization) and the near-collinear nature of all the P-Ir-Ir-Au-P^{3+} bond vectors. Better propagation of nuclear spin through Au may acount for the larger P-P coupling in **2** despite the fact that the P-P internuclear

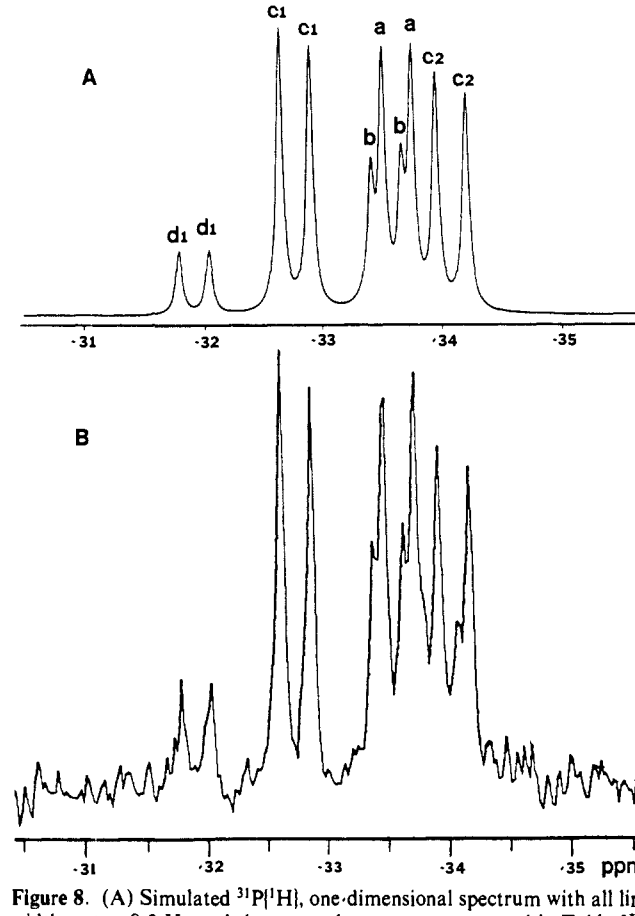

Figure 8. (A) Simulated $^{31}P\{^1H\}$, one-dimensional spectrum with all line widths set to 8.0 Hz and the spectral parameters reported in Table III. (B) Experimental one-dimensional 121.5-MHz $^{31}P\{^1H\}$ spectrum of $[Ir_2(dimen)_4(PPh_3)Au(PPh_3)](PF_6)_3$ in CH_2Cl_2 taken at 27 °C.

distance in **2** P-Ir-Ir-Au-P^{3+} [10.242 (7) Å] is slightly longer than the P-P distance in P-Ir-Ag-Ir-P^{3+} [10.06 (3) Å].

The chemical shifts of the Ir-P phosphorus atoms of isomers A and B (the 2:2 cis and trans isomers) of -33.62 and -33.53 ppm, respectively, are close to the average Ir-P chemical shift of the 3:1 isomers, C1 and C2 (-33.42 ppm). This phenomenon is consistent with that found in P-Ir-Ag-Ir-P^{3+}. The phosphorus chemical shifts in P-Ir-Ag-Ir-P^{3+} lie within an appropriate 2 ppm window, which is similar to the chemical shift range of the Ir-P multiplet in **2** and is apparently a stronger function of the steric interaction at the iridium site. In support of this thesis, the Au-P phosphorus resonances in **2** (one bond further removed from the iridium) show a smaller chemical shift window of only 0.5 ppm. The simulation of the Au-P multiplet was not undertaken because the resonances severely overlap in the narrower chemical shift

window; however, three average 30.3-Hz couplings are observed between six distinct peaks in the multiplet. The sharpness of the individual peaks in both the Au–P and Ir–P multiplets indicates fluxional processes that involve dissociation of triphenylphosphine from Ir and Au are slow on the NMR time scale at 298 K.

(b) Assignment of the ^{31}P NMR Spectrum of 1. As observed for **2**, a complex pattern is seen in the PPh_3 region of the one-dimensional $^{31}P\{^1H\}$ NMR solution spectrum of the silver analogue, $[Ir_2(dimen)_4(PPh_3)Ag(PPh_3)](PF_6)_3$, at room temperature. The broadening of the individual resonances indicated that some chemical exchange occurs at room temperature, and suggested that sharper spectra could be obtained at low temperature. In the low-temperature (−40 °C) spectrum,[49] exchange is stopped and the spectrum shows the same general spectral features as **2** with the added complexity of ^{107}Ag and ^{109}Ag coupling. The two downfield multiplets centered at 11.9 ppm are the $Ag(PPh_3)^+$ phosphorus signals coupled to ^{107}Ag and ^{109}Ag with one-bond Ag–P couplings of approximately 500 Hz. The multiplet at −37.3 ppm is due to the Ir–P resonance, close to the average chemical shift of the $Au(PPh_3)$ resonances in **2** (−33.2 ppm). In general, each chemically distinct P–Ag unit exhibits a characteristic ^{31}P resonance.

The doublet of doublets pattern is due to unequal ^{31}P–^{107}Ag and ^{31}P–^{109}Ag couplings in the molecule. ^{107}Ag and ^{109}Ag occur in 51.35 and 48.65% natural abundance, and both have $I = {}^1/_2$. ^{109}Ag is responsible for the larger coupling, and the ratio of ^{109}Ag–P to ^{107}Ag–P coupling is theoretically equal to 1.149, the ratio of their gyromagnetic moments.[50,51] The average one-bond ^{109}Ag–P coupling in **1** is 512 Hz, and the ^{107}Ag–P coupling is 440 Hz to give a ^{109}Ag–P/^{107}Ag–P ratio of 1.16, in good agreement with the theoretical prediction. Coupling constants on the order of 500 Hz are normal values for one-bond Ag–P couplings.[47,48] Due to the small magnitude of the Ag–P couplings, for the Ir–P unit, the different ^{107}Ag and ^{109}Ag coupling constants are not resolvable.

The simulated ^{31}P NMR spectrum of **1** closely matches the one-dimensional ^{31}P spectrum.[51] Table III lists the spectral parameters used for the simulation. A major difference between spectra simulated for the silver and gold outside adducts is that the chemical shifts of isomers A and B of the silver adduct are identical. The degeneracy of A and B produces only four sets of peaks for **1**, while five sets of peaks are present for **2**. As previously observed in the outside gold adduct **2**, the larger set of peaks at −36.89 ppm is assigned to the C1 isomer because the triphenylphosphine ligand bonded to the iridium atom in this isomer has fewer steric interactions with the dimen methyl groups than the C2 isomer. On the basis of this assignment, the ^{31}P spectrum predicts C1 is preferentially formed in a 2:1 ratio (rather than the predicted 1:1 statistical ratio) over C2 based on the relative peak areas. The remaining set of four peaks centered at −36.21 ppm is assigned to the 4:0 isomer, D1. The relative experimental integration of the peak centered at −36.21 ppm (0.153) approximates the statistical value (1/8 or 0.125) if the only 4:0 isomer formed as D1 is the isomer.

Conclusions

Complexes of the form $[Ir_2(dimen)_4(PPh_3)M(PPh_3)](PF_6)_3$ (where M = Ag, Au) exhibit a considerable degree of isomerism due to the head-to-tail isomerism of the parent $[Ir_2(dimen)_4]^{2+}$ complex and the additional axial site differences generated. In the crystal of **2** (M = Au), two of the possible six isomers (A and C2) are present as a disordered pair. The slight broadening of the ^{31}P signals of all the isomers present at room temperature in solutions of **1** (M = Ag) indicated that slow ligand exchange of PPh_3 occurs. The ^{31}P NMR studies also indicate that for both **1** and **2** the most sterically hindered isomer (D2), which has PPh_3 directly bound in the axial position to the more congested Ir atom, is not appreciably formed in solution. The second most hindered isomer (C2) is present in solutions but is slightly depleted relative to the more stable C1 isomer. This effect is accentuated for the Ag compound.

In the future, we plan to investigate the potential isomerization of **1** and **2** to the corresponding encapsulated adducts and we plan to attempt at least a partial separation and purification of the isomers we have observed in this system.

Acknowledgment. We thank Doyle Britton and Steve Philson for several stimulating discussions and Johnson-Matthey, Inc. for generous loans of iridium trichloride.

Supplementary Material Available: ^{31}P NMR spectra and tables for the positional parameters, selected distances and angles of the PF_6^- and CH_3CN groups, selected least-squares planes, and anisotropic temperature factors for **1** (19 pages); observed and calculated structure factors for **1** (44 pages). Ordering information is given on any current masthead page.

(49) Please see supplementary material.
(50) Muetterites, E. L.; Alegranti, C. W. *J. Am. Chem. Soc.* **1970**, *92*, 4114.
(51) Muetterites, E. L.; Alegranti, C. W. *J. Am. Chem. Soc.* **1972**, *94*, 6386.